Assessment of a non-conservative Residual Distribution scheme for solving a four-equation two-phase system with phase transition

Paola Bacigaluppi, Julien Carlier, Marica Pelanti, Pietro Marco Congedo, Rémi Abgrall

Noname manuscript No.
(will be inserted by the editor)

Assessment of a non-conservative Residual Distribution scheme for solving a four-equation two-phase system with phase transition

Paola Bacigaluppi · Julien Carlier · Marica Pelanti · Pietro Marco Congedo · Rémi Abgrall

Received: date / Accepted: date

Abstract This work focuses on a four-equation model for simulating two-phase mixtures with phase transition. The main assumption consists in a homogeneous temperature, pressure and velocity fields between the two phases. In particular, we tackle the study of time dependent problems with strong discontinuities and phase transition. This work presents the extension of a non-conservative residual distribution scheme to solve a four-equation two-phase system with phase transition. This non-conservative formulation allows avoiding the classical oscillations obtained by many approaches, that might appear for the pressure profile across contact discontinuities. The proposed method relies on a Finite Volume based Residual Distribution scheme which is designed for an explicit second-order time stepping. We test the non-conservative Residual Distribution scheme on several benchmark problems and assess the results via a cross-validation with the approximated solution obtained via a conservative approach, based on an HLLC solver. Furthermore, we check both methods for mesh convergence and show the effective robustness on very severe test cases, that involve both problems with and without phase transition.

Keywords Non-conservative formulation · hyperbolic problems · compressible flows · multiphase flows · phase transition · Residual Distribution scheme · Godunov method · diffuse interface model

P. Bacigaluppi, R. Abgrall
Institute of Mathematics, University of Zurich, Switzerland
E-mail: paola.bacigaluppi@gmail.com, remi.abgrall@math.uzh.ch

J. Carlier, M. Pelanti
ENSTA ParisTech, France

P.M. Congedo
Inria, Centre des Mathématiques Appliquées, Ecole Polytechnique, France

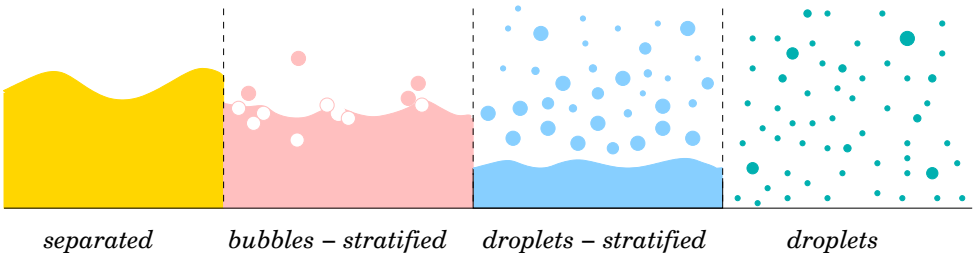

Fig. 1 Schematic representation of different typologies of two-phase flows.

1 Introduction

In many different engineering applications, as for steam turbines, turbo-pumps or trilateral flash cycles, as well as for engines, or wings, we encounter multiphase flows. These flows are extremely difficult to characterize and show sometimes a very peculiar behaviour as phase transition. To study the behaviour in different operating conditions, experimental approaches are very common, but are highly expensive and, therefore, numerical simulations are desirable to get an initial prediction of the physical behaviour which might be encountered.

Among the mathematical models used in the multiphase community, some are based on the reinterpretation of the Euler equations with some additional source term. In particular, one may refer to the Baer-Nunziato seven-equation model, first presented in [9], from which several methods, with higher or lower complexity according to the physics aimed to be represented, have been derived (see [18]). The present work is based on these diffuse interface models, and in particular considers a reduced version of the Baer-Nunziato model, namely a four-equation model, where the reduction from the original seven-equation model comes from the assumption of considering that there is a very large interface between two different phases, such that the velocity, pressure and temperature of one phase coincide with those of the other media. This assumption is used, for example, in case the study concerns fog, which can be seen as a stratified two phase flow (see cf. Figure 1), or cavitation, which is an extremely violent implosive/explosive process.

This model is characterized by a thermo-chemical non-equilibrium, i.e. the involved flows undergo a mass transition. Nevertheless, it is worth to remark, that the considered model is not able to simulate metastable states (see Fig. 2), due to the already mentioned assumption of temperature equilibrium. Moreover, one should not confuse the model used in this paper with a similar model which was introduced in [15] and is the so-called Homogeneous Relaxation Method (HRM).

For solving the proposed four-equation system, we rely on a non-conservative formulation of the Residual Distributions Finite Volume type technique (RD) and cross-validate it with a more standard HLLC solver tailored for the conservative formulation of the considered model. The proposed scheme aims at bringing together different approximating strategies presented in previous papers, as [4,7,5,8]. Indeed, the discretization is based on a second-order predictor-correction method as presented in

[21,4,7,1]. Following the work of Abgrall et al. [5], the considered system is rewritten in terms of a non-conservative formulation of the internal energy equation which is approximated in such a way, that the conservation is guaranteed. The idea behind the choice of a non-conservative formulation, as seen in [5], is due to the many advantages, especially for engineering applications, which are represented by the possibility to work directly with quantities, such as pressures or internal energies instead of having them derived from the total energy. Indeed, when coming, for example, across contact discontinuities, the velocity and the pressure do not change, while the density does. Deriving the internal energy or pressures from the total energy, may, therefore, not be completely accurate from a numerical point of view. Further, another relevant advantage is represented by the possibility of dealing easily with non-linear equations of state, as for example the family of Mie-Grüneisen equations of state. To ensure a good approximation throughout the discontinuities, the so-called Multi-dimensional Optimal Order Detection (MOOD) limiting of [8] has been applied, in order to switch from a second-order of accuracy to a first-order in case of numerical oscillations, or in case of computational issues, such as the appearance of NaN or InF.

In the following, we first introduce in Section 2 the mathematical model and recall the non-conservative formulation used to approximate the hyperbolic part of the considered system of equations. We then describe the Residual Distribution scheme and the treatment of the source terms accounting for the mass transition in Section 3. Finally, in Section 4 we briefly mention the Harten-Lax-van Leer-Contact (HLLC) approximate Riemann solver implemented for solving the conservative formulation of the four-equation model. In Section 5, several significant benchmark problems cross-validate the chosen mathematical model and show the numerical validity of the Finite Volume based Residual Distribution scheme. Some conclusions and perspectives are drawn in Section 6.

2 Four-equation Model

The four-equation model is a simplified version of the Baer-Nunziato two-phase model [9]. It consists of one mass equation for each phase k and a momentum and energy equation for the mixture:

$$\begin{cases} \frac{\partial(\alpha_1\rho_1)}{\partial t} + \text{div}\,(\alpha_1\rho_1\,\mathbf{u}) = \Gamma \\ \frac{\partial(\alpha_2\rho_2)}{\partial t} + \text{div}\,(\alpha_2\rho_2\,\mathbf{u}) = -\Gamma \\ \frac{\partial(\rho_{tot}\,\mathbf{u})}{\partial t} + \text{div}\,(\rho_{tot}\;\mathbf{u}\otimes\mathbf{u} + PId) = 0 \\ \frac{\partial E_{tot}}{\partial t} + \text{div}\;(E_{tot}+P)\,u = 0. \end{cases} \tag{1}$$

The non-conservative formulation of (1) reads

$$\begin{cases} \frac{\partial(\alpha_1\rho_1)}{\partial t} + \text{div}\,(\alpha_1\rho_1\,\mathbf{u}) = \Gamma \\ \frac{\partial(\alpha_2\rho_2)}{\partial t} + \text{div}\,(\alpha_2\rho_2\,\mathbf{u}) = -\Gamma \\ \frac{\partial(\rho_{tot}\,\mathbf{u})}{\partial t} + \text{div}\,(\rho_{tot}\;\mathbf{u}\otimes\mathbf{u} + PId) = 0 \\ \frac{\partial e_{tot}}{\partial t} + \mathbf{u}\cdot\nabla e_{tot} + (e_{tot}+P)\,\text{div}\,\mathbf{u} = 0, \end{cases} \tag{2}$$

where ρ_k and α_k represent for each phase the density and the volume fraction, respectively. The liquid (gaseous) phase is denoted by subscript l or 1 (g or 2). Here $\mathbf{u}$ represents the velocity, ρ_{tot} the mixture density, P the pressure and c_{tot} the mixture speed of sound. The Wood velocity $\frac{1}{\rho_{tot}c_{tot}^2} = \frac{\alpha_l}{\rho_l c_l^2} + \frac{\alpha_g}{\rho_g c_g^2}$ describes the total sound speed, where

$$c_k^2 = \left(\frac{\partial P_k}{\partial \rho_k}\right)\Big|_{s_k} \tag{3}$$

is the squared speed of sound for phase k, and s_k the entropy for phase k.
The volume fraction α_k has to fulfil the requirement

$$\sum_k \alpha_k = 1. \tag{4}$$

We define the total energy as

$$E_{tot} = e_{tot} + \frac{1}{2}\rho_{tot}\mathbf{u}^2, \tag{5}$$

with the total internal energy $e_{tot} = \sum_k \alpha_k e_k$, where e_k is the internal energy of phase k. The mass transfer term Γ is equal to $\Gamma = \theta(\nu_l - \nu_g)$ with ν the chemical potentials (Gibbs function) of the gaseous and liquid media, while θ represents the relaxation time of the process at which the thermodynamic equilibrium is reached (which enables the fulfillment of entropy inequality).

In certain communities, this model is referred to as Homogeneous Relaxation Model (HRM). Nevertheless, the thermodynamic assumptions behind the models (1)-(2) are different from the original HRM model of Downar [15], which does not assume a temperature equilibrium. Further, the original HRM model can also account for *metastable states*, which are those identified when at the final pressure, the temperature is higher w.r.t. the saturated temperature (see Figure 2). This situation occurs, for example, when a liquid that is initially in thermodynamic equilibrium experiences a strong rarefaction. To reach the equilibrium of temperature, the flow either produces at high velocities an evaporating (pure vapour) front or developes a liquid-vapor mixture ([23]).

The thermodynamic closure for (1)-(2) reads

$$\begin{cases} T_l = T_g = T \\ e_{tot} = \alpha_l e_l + \alpha_g e_g \\ P_l = P_g = P \\ \alpha_l + \alpha_g = 1. \end{cases} \tag{6}$$

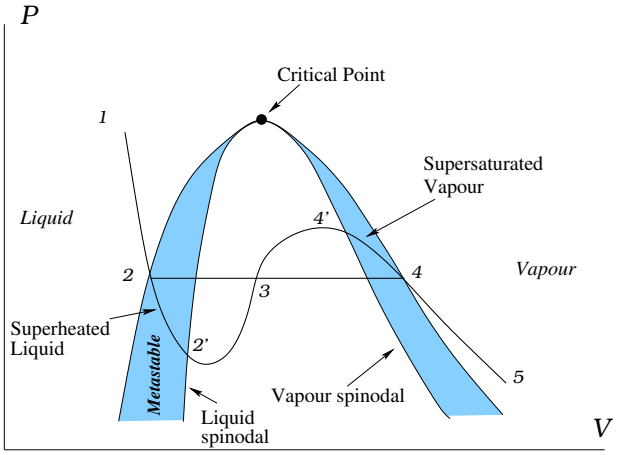

Fig. 2 Generic pressure-volume diagram showing the metastable state

Here T_k represents the temperature for each phase k. In the following, we consider stiffened equations of state (EOS) for each phase k, that is given by the following main relations:

$$\begin{cases} P_k(\rho_k, e_k) = (\gamma_k - 1)(e_k - \rho_k\, q_k) - \gamma_k\, P_{\infty,k} \\ c_k(P_k, \rho_k) = \sqrt{\gamma_k \frac{P_k + P_{\infty,k}}{\rho_k}} \\ T_k(P_k, \rho_k) = \frac{P_k + P_{\infty,k}}{\rho_k c_{v_k}\,(\gamma_k - 1)} \\ e_k(P_k, T_k) = \rho_k \frac{P_k + \gamma_k\, P_{\infty,k}}{P_k + P_{\infty,k}} c_{v_k}\, T_k + \rho_k q_k \\ g_k(P_k, T_k) = (\gamma_k\, c_{v_k} - q_k^{'}) T_k - c_{v_k} T_k ln \left[\frac{T_k^{\gamma_k}}{(P_k + P_{\infty,k})^{\gamma_k - 1}} \right] + q_k \\ \tau_k = \frac{(\gamma_k - 1) c_{v_k} T_k}{P_k + P_{\infty,k}} \end{cases} \tag{7}$$

Here, for completeness we mention that the polytropic coefficient γ_k is the constant ratio of specific heat capacities of phase k, while c_{v_k} and $P_{\infty,k}$ are respectively the specific heat at constant volume and a constant reference pressure for phase k. The specific energy of the fluid at a given reference state for phase k is denoted by q_k, while $\tau_k = \frac{1}{\rho_k}$ corresponds to the specific volume .

The mixture temperature reads

$$T(P, \alpha_l, \rho_{tot}) = \left(\frac{\alpha_l \rho_l c_{v_l}\,(\gamma_l - 1)}{P + P_{\infty,l}} + \frac{(1 - \alpha_l)\rho_g c_{v_g}\,(\gamma_g - 1)}{P + P_{\infty,g}} \right)^{-1} \tag{8}$$

while the mixture internal energy is

$$\begin{aligned} e_{tot}(T, P, \alpha_l) = & \alpha_l \rho_l \left(c_{v_l}\, T \frac{P + \gamma_l\, P_{\infty,l}}{P + P_{\infty,l}} + q_l \right) \\ & + (1 - \alpha_l)\rho_g \left(c_{v_l}\, T \frac{P + \gamma_g\, P_{\infty,g}}{P + P_{\infty,g}} + q_g \right). \end{aligned} \tag{9}$$

As for the pressure, we consider

$$P(e,\alpha_l,\rho_{tot}) = \frac{1}{2}(A_l + A_g - (P_{\infty,l} + P_{\infty_g})) + \sqrt{\frac{1}{4}(A_g - A_l - (P_{\infty,g} - P_{\infty,l}))^2 + A_l\, A_g}, \tag{10}$$

where

$$A_k = \frac{\rho_k \alpha_k (\gamma_k - 1) c_{v_k}}{\rho_l \alpha_l c_{v_l} + \rho_g (1-\alpha_l) c_{vg}} \Big(e_{tot} - (\alpha_l\, \rho_l\, q_l + (1-\alpha_l)\, \rho_g\, q_g) - P_{\infty,k} \Big). \tag{11}$$

Finally, the mixture sound speed considered for this set of equations is given by [16] and reads

$$\begin{aligned} c_{tot}^2 =& \frac{1}{2}\Big([e_{tot} - (Y_l q_l + Y_g q_g)]\,(a_1 + a_2) + \frac{\frac{1}{2}\left(\frac{\partial R_1}{\partial \rho_{tot}}\right)_{e_{tot}} + \left(\frac{\partial R_2}{\partial \rho_{tot}}\right)_{e_{tot}}}{\sqrt{\frac{1}{4}R_1 R_1 + R_2}} \\ &+ \frac{P}{\rho_{tot}^2}\Big(\rho_{tot}(a_1 + a_2) + \frac{\frac{1}{2}\left(\frac{\partial R_1}{\partial e_{tot}}\right)_{\rho_{tot}} + \left(\frac{\partial R_2}{\partial e_{tot}}\right)_{\rho_{tot}}}{\sqrt{\frac{1}{4}R_1 R_1 + R_2}} \Big)\Big), \end{aligned} \tag{12}$$

with

$$a1 = \frac{Y_l(\gamma_l - 1)c_{v_l}}{Y_l c_{v_l} + Y_g c_{v_g}}, \qquad a2 = \frac{Y_g(\gamma_g - 1)c_{v_g}}{Y_l c_{v_l} + Y_g c_{v_g}}$$

and

$$\begin{aligned} R1 &= a_2 \rho_{tot}[e_{tot} - (Y_l q_l + Y_g q_g)] - a_2 P_{\infty,g} - a_1 \rho_{tot}[e_{tot} - (Y_l q_l + Y_g q_g)] + a_1 P_{\infty,l} - P_{\infty,g} + P_{\infty,l} \\ R2 &= a_2 a_1 (\rho_{tot}[e_{tot} - (Y_l q_l + Y_g q_g)] - P_{\infty,l})(\rho_{tot}[e_{tot} - (Y_l q_l + Y_g q_g)] - P_{\infty,g}). \end{aligned} \tag{13}$$

$Y_k = \frac{\alpha_k \rho_k}{\rho_{tot}}$ denotes the mass fraction with $\sum_k Y_k = 1$. We remark, that within this model, as usually done in the context of Baer-Nunziato type systems, the "pure" phase always contains a small amount of the other phase, s.t. $\alpha_k = 1 - \varepsilon$, with $\varepsilon \approx 10^{-6}$, due to technicalities.

In [10], the authors have compared formula (12) with the one of Wood (3). As shown in Figure 3, the approximations display a similar behaviour, whereas the sound speed due to Wood results to have higher values in the equilibrium area. Since this system does not consider directly the volume fractions, it is actually more straightforward to apply the approximation given by (12), than the formula (3).

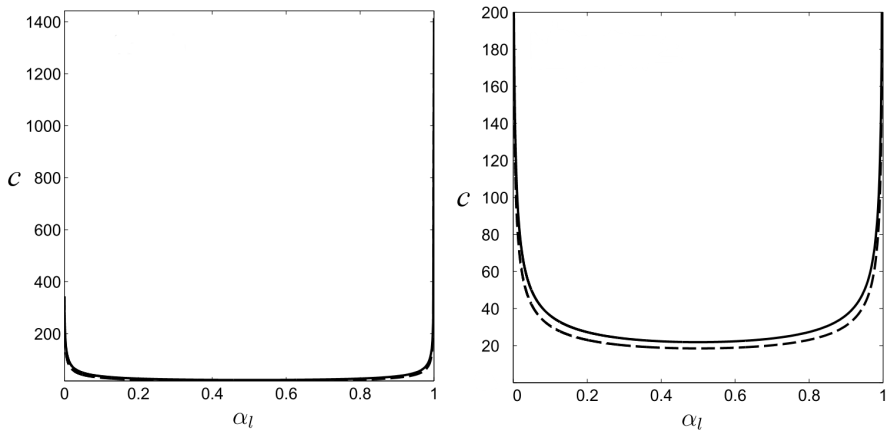

Fig. 3 Comparison between (3) (continuous line) and (12) (dashed line), for $\rho_{air} = 1\ kg/m^3$, $c_{air} = 374\ m/s$, $\rho_{water} = 1000\ kg/m^3$ and $c_{water} = 1568\ m/s$ and the phase values according to Table 1. The right picture is a zoom of the left one.

3 Non-conservative Second-Order Explicit Residual Distributions Scheme

The numerical approximation considered within this work follows the idea to solve the presented four-equation pressure- and temperature-equilibrium system via a splitting method, which takes first into account only the hyperbolic problem given by (14) and then adds the source terms, such that the solution is updated with the mass transition of the phases as (15).

$$\begin{cases} \partial_t(\alpha_1\rho_1) + \text{div}\,(\alpha_1\rho_1\,\mathbf{u}) = 0 \\ \partial_t(\alpha_2\rho_2) + \text{div}\,(\alpha_2\rho_2\,\mathbf{u}) = 0 \\ \partial_t(\rho_{tot}\,\mathbf{u}) + \text{div}\,(\rho_{tot}\ \ \mathbf{u}\otimes\mathbf{u} + PId) = 0 \\ \partial_t e_{tot} + \mathbf{u}\cdot\nabla e_{tot} + (e_{tot}+P)\,\text{div}\,\mathbf{u} = 0 \end{cases} \tag{14}$$

$$\begin{cases} \partial_t \alpha_1\rho_1 = \Gamma \\ \partial_t \alpha_2\rho_2 = -\Gamma \\ \partial_t \rho_{tot}\mathbf{u} = 0 \\ \partial_t e_{tot} = 0 \end{cases} \tag{15}$$

In the 1D case, the set of equations (14) can be rewritten as

$$\begin{cases} \partial_t U + \text{div}\,\mathbf{F}(U) = 0 \\ \partial_t e_{tot} + \mathbf{u}\cdot\nabla e_{tot} + (e_{tot}+P)\text{div}\,\mathbf{u} = 0 \\ U(x,0) = U^0(x), \end{cases} \tag{16}$$

on $\Omega \times [0,T]$, with $U = [\alpha_1\rho_1,\ \alpha_2\rho_2,\ \rho_{tot}\mathbf{u}]^T$ and with the flux defined as

$$\mathbf{F}(U) = (\alpha_1\rho_1 u,\ \alpha_2\rho_2 u,\ \rho_{tot}\ \mathbf{u}\otimes\mathbf{u} + PId)^T.$$

3.1 Approximation of the Hyperbolic part

Inspired by the work of [21], [7] and [4], we have designed the discretiztion in time for (14) with a second-order explicit (Runge-Kutta) method. This time-stepping approach is used in combination with the Residual Distribution discretization in space, which has been accurately presented in some recent work [1,8].

Let us start by splitting the spatial domain Ω in N_e conformal non-overlapping elements with characteristic length Δx or h, and denote the set of all the elements by Ω_h, as for example in Figure 4. K refers to a generic element of the tessellation Ω_h, and $\Gamma = \partial\Omega_h$ represents the boundary of the domain's problem.

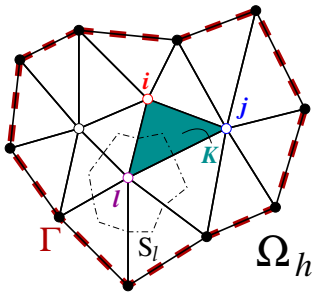

Fig. 4 Discretized domain Ω_h and its boundary Γ for two dimensions ($d = 2$) and simplexes.

Within each time step $[t_n, t_{n+1}]$ we consider M subintervals, so that $t_n = t_{n,0} < t_{n,1} < \cdots < t_{n,m} < \cdots < t_{n,M} = t_{n+1}$. Next, for each subinterval $[t_{n,m}, t_{n,m+1}]$, we denote the approximated solution at the m-th substep $t_{n,m}$ as $U_h^{n,m}$ and the solution at t_n as U_h^n.

The proposed time-stepping is recast as a predictor-corrector approximation with $M = 2$. For any degree of freedom $\sigma \in K$ we have an

- initialization: $U_\sigma^{(n,1)} = U_\sigma^{(n,0)} = U_\sigma^n$;
- loop for $m = 0, 1$:

$$|S_\sigma| \frac{U_\sigma^{(n,m+1)} - U_\sigma^{(n,m)}}{\Delta t_{n,m}} + \sum_{K|\sigma\in K} \phi_\sigma^K(U_h^{(n,m)}, U_h^{(n,0)}) = 0, \tag{17}$$

where ϕ_σ^K is a so-called nodal residual which is detailed in the next paragraph and $|S_\sigma|$ is the area of the median dual cell S_σ obtained by joining the gravity centres of the cells with the midpoints of the edges meeting in the node σ (see cf. [13] and Figure 4).

The idea of the prediction step is thus to be first order accurate and to be given by a flux difference. The second-order in time is then achieved with the correction step, which takes the obtained prediction approximation as the previous sub-timestep solution. The second-order in space is guaranteed by a correct choice of the nodal residual term ϕ_σ^K.

In the next paragrphs, we provide details on the actual choice of ϕ_σ^K (cf. Section 3.2) and the conservative approach for the treatment of the non-conservative formulation of system (14) (cf. Section 3.3).

3.2 Optimization via an "A Posteriori" Limiting

It is well known that in literature several benchmark problems related to multiphase flow systems are extremely difficult to be reproduced as they require an extreme robustness of the scheme. This might be the case, for example, when very high gradients of pressures or velocities are defining the set-up of the problem. On one hand, a highly accurate scheme with little or no dissipation mechanisms has the drawback to not allow for the required robustness across strong interacting discontinuities for benchmark problems designed for extremely severe initial conditions. On the other hand, adopting a dissipative, first order formulation would not allow to retrieve the desired accuracy in smooth regions. To overcome these outlined issues, we consider the proposed scheme of [8], which combines different numerical scheme to retrieve high accuracy in smooth regions of the flow, while, at the same time, ensuring robustness and a non-oscillatory behaviour in regions of steep gradients. This idea, as mentioned previously, is also known as the Multidimensional Optimal Order Detection (MOOD) approach ([11], [14]) and allows to introduce local dissipation if needed. Nevertheless, this strategy differs from those well known available in literature, as shall explained in the following. We consider ϕ_σ^K of equation (17) rewritten as

$$\phi_\sigma^{K,s}(U) = \int_K \varphi_\sigma \partial_t U_\sigma \, d\mathbf{x} + \phi_{\sigma,\mathbf{x}}^{K,s}(U), \tag{18}$$

where we have dropped for simplicity the subscripts denoting the time dependency, s.t. $\phi_\sigma^{K,s}(U) = \phi_\sigma^{K,s}(U_h^{(n,m)}, U_h^{(n,0)})$.

In the following we consider a Finite Element-based approach, but it has been shown in [2] that residual based configurations may be rewritten in terms of Finite Volumes or Discontinuous Galerkin schemes.
Considering a finite element type setting, we thus consider our approimation space to be given by globally continous piecewise polynomials of degree k, s.t. $V_h = \{U \in C^0(\Omega_h), U|_K \in \mathscr{P}^k, \forall K \in \Omega_h\}$. The φ_σ in (18) denotes a basis function of choice, as, for instance, given by Lagrangian polynomials, and such that $U_h = \sum_{K\in\Omega_h}\sum_{\sigma\in K} U_\sigma \varphi_\sigma \Big|_K$.

The optimization strategy is designed for the current work as follows:

1. For each degree of freedom $\sigma \in K$ we start with the solution at time t_n and

2. compute the candidate solution $U_h^{K,s,n+1}$ for time t_{n+1}.
3. The candidate solution is checked over a series of admissibility criteria, as listed in Section 3.2.3.
   a) If the candidate solution does not fullfill one of the criteria in a cell K, we use locally on the troubled cell a more dissipative scheme, repeating steps 2-3. We go to step 4, in case we have reached a "parachute" scheme, typically of first order of accuracy.
   b) If the candidate solution does fullfill all the set admissibility criteria, we go to step 4.
4. We accept our candidate solution to be $U_h^{K,n+1} = U_h^{K,s,n+1}$.

In this work we loop three times over the steps 3-4, i.e. we consider in total three different schemes, $s = 0,1,2$, including the parachute scheme to compute our candidate solution. At every violation of the admissibility criteria we impose $s = s-1$ locally on the troubled cell. The scheme considered in this work are

– $s = 2$: "stabilized Galerkin scheme"

$$\phi_{\sigma,\mathbf{x}}^{K,2}(U) = \int_{\partial K} \varphi_\sigma \mathbf{F}(U)\cdot\mathbf{n}\, d\Gamma - \int_K \nabla\varphi_\sigma \cdot \mathbf{F}(U)\, d\mathbf{x} + \phi_{\sigma,\mathbf{x}}^{K,Jump}(U) \tag{19}$$

– $s = 1$: "stabilized, blended Rusanov scheme"

$$\phi_{\sigma,\mathbf{x}}^{K,1}(U) = \phi_{\sigma,\mathbf{x}}^{K,\star}(U) + \phi_{\sigma,\mathbf{x}}^{K,Jump}(U), \tag{20}$$

with $\phi_{\sigma,\mathbf{x}}^{K,\star}(U)$ defined in paragraph 3.2.2.

– $s = 0$: "Rusanov scheme"

$$\phi_{\sigma,\mathbf{x}}^{K,0}(U) = \int_{\partial K} \varphi_\sigma \mathbf{F}(U)\cdot\mathbf{n}\, d\Gamma - \int_K \nabla\varphi_\sigma \cdot \mathbf{F}(U)\, d\mathbf{x} + \alpha(\widetilde{U_\sigma} - \overline{U}^K). \tag{21}$$

See paragraph 3.2.1 for a comment on the terms.

The stabilization for $s = 1,2$ is expressed as $\phi_{\sigma,\mathbf{x}}^{K,Jump}(U) = \theta h_e^2 \int_e [\nabla U]\cdot[\nabla\varphi_\sigma]\, d\Gamma$.

3.2.1 A comment on the Rusanov scheme ($s = 0$)

The Rusanov's scheme, also known as the local Lax-Friedrich's scheme, is in our case the parachute scheme, i.e. a first order approach. In particular it considers in our predictor-corrector approach the $\widetilde{U_\sigma} = \frac{U_\sigma^{n,m} + U_\sigma^{n,0}}{2}$ and $\overline{U}^K = \frac{1}{N_{DoF}}\Big(\sum_{\sigma\in K} \frac{1}{2}\big(U_\sigma^{n,m} + U_\sigma^{n,0}\big)\Big)$. Here N_{DoF} represents the number of degrees of freedom within one cell K. Further, α_K allows to add numerical diffusion to the approximation in order to guarantee a monotone solution and is in the form of a characteristic velocity written as

$$\alpha_K = \max_{\sigma\in K}\left(\rho_S\Big(\nabla_U \mathbf{F}(U_h)\cdot\nabla\varphi_\sigma\Big)\right).$$

To determine the spectral radius $\rho_S\Big(\nabla_U \mathbf{F}(U_h)\cdot\nabla\varphi_\sigma\Big)$ within a cell, we have used the arithmetic averages over one cell, such that $\alpha_K = max(|\lambda_\sigma^K(\widetilde{U}_\sigma)|)$. Note that λ_σ^K represents the eigenvalues of the system.

3.2.2 A comment on the stabilized, blended Rusanov scheme ($s = 1$)

For the sake of allowing the reproducibility of the presented method, we detail hereafter the technical choices behind the stabilized, blended Rusanov scheme ($s = 1$). To do so, we will in the following denote $\phi^{K,0}_{\sigma,\mathbf{x}}(U)$ as $\phi^{K,Rus}_{\sigma,\mathbf{x}}(U) = \phi^{K,Rus}_{\sigma,\mathbf{x}}(U^{(n,m)}_h, U^{n,0}_h)$, to avoid any possible misunderstanding. Scheme $s = 1$ considers a blending of the Rusanov scheme that allows for second-order accuracy. This relies on the decomposition in local characteristic variables of the first-order residuals such that, instead of $\phi^{K,Rus}_{\sigma,\mathbf{x}}(U)$, one considers $\phi^{K,\star}_{\sigma,\mathbf{x}}(U)$.
To compute $\phi^{K,\star}_{\sigma,\mathbf{x}}(U)$, we proceed as follows.

- We first consider the definition of the residual according to equation (21)
- Then we consider the eigen-decomposition of $\mathbf{A_n} = \mathbf{A}(\widehat{U}_K)n_x + \mathbf{B}(\widehat{U}_K)n_y$ (in 2D, while in 1D it would simply be $\mathbf{A}(\widehat{U}_K)$. The matrices $\mathbf{A}$ and $\mathbf{B}$ are the Jacobians of the x- and y- component of the flux $\mathbf{F}$ with respect to the state $\widehat{U}_K$. Here, the vector $\mathbf{n}$ is a unit vector in the direction of the velocity field when it is nonzero, or any arbitrary direction otherwise. Of course, this direction is not relevant in one dimension. The right eigenvectors of $\mathbf{A_n}$ are denoted by $\{\mathbf{r}_\xi\}$. We denote by $\{\ell_\xi\}$ the left eigenvectors of $\mathbf{A_n}$, so that any state X can be written as: $X = \sum_\xi \ell_\xi(X)\mathbf{r}_\xi$.
- Then we decompose, for any degree of freedom σ:

$$\phi^{K,Rus}_{\sigma,\mathbf{x}}(U) = \sum_\xi \ell_\xi\big(\phi^{K,Rus}_{\sigma,\mathbf{x}}(U)\big)\mathbf{r}_\xi$$

  We note that for any ξ,

$$\ell_\xi\big(\phi^K_{\mathbf{x}}\big) = \sum_{\sigma\in K} \ell_\xi\big(\phi^{K,Rus}_{\sigma,\mathbf{x}}(U)\big),$$

  where $\phi^K_{\mathbf{x}} = \sum_{\sigma\in K}\phi^{K,Rus}_{\sigma,,\mathbf{x}}$ is the total residual.
- The next step is to define $\phi^{K,\star}_{\sigma,\mathbf{x}}(U)$ as:

$$\phi^{K,\star}_{\sigma,\mathbf{x}}(U) = \sum_\xi \ell^\star_\xi\big(\phi^K_{\sigma,\mathbf{x}}\big)\mathbf{r}_\xi \tag{22a}$$

  where:

$$\ell^\star_\xi\big(\phi^K_{\sigma,\mathbf{x}}\big) = (1-\Theta_\xi)\overline{\phi}^{K,Rus}_{\sigma,\mathbf{x}}(U) + \Theta_\xi\ell_\xi\big(\phi^{K,Rus}_{\sigma,\mathbf{x}}(U)\big) \tag{22b}$$

  with

$$\Theta_\xi = \frac{\big|\ell_\xi\big(\phi^{K,Rus}_{\sigma,\mathbf{x}}(U)\big)\big|}{\sum_{\sigma'\in K}\big|\ell_\xi\big(\phi^{K,Rus}_{\sigma',\mathbf{x}}(U)\big)\big|} \tag{22c}$$

  and

$$\overline{\phi}^{K,Rus}_{\sigma,\mathbf{x}}(U) = \frac{\max\Big(\frac{\ell_\xi\left(\phi^{K,Rus}_{\sigma,\mathbf{x}}(U)\right)}{\ell_\xi\left[\phi^K_{\mathbf{x}}\right]},0\Big)}{\sum_{\sigma'\in K}\max\Big(\frac{\ell_\xi\left(\phi^{K,Rus}_{\sigma',\mathbf{x}}(U)\right)}{\ell_\xi\left[\phi^K_{\mathbf{x}}\right]},0\Big)} \tag{22d}$$

  Note that $\Theta_\xi \in [0,1]$. This guarantees that the scheme is second-order in time and space and (formally) non-oscillatory, see [21,3,6] for more details.

3.2.3 Detection procedure for the "a posteriori" limiting

The detection criteria responsible to mark the approximation as acceptable are based on physical/modelling and numerical considerations. The cell will be thus flagged as 'good' if its candidate solution fulfils all detection criteria and it is not a direct neighbour of a bad cell. These criteria reads

$$\mathscr{B} = \left\{ K \in \Omega_h, \text{ s.t. } (\mathrm{PAD}_K \times \mathrm{CAD}_K \times \mathrm{P}_K \times \mathrm{NAD}_K = 1) \text{ or } \left(\exists K' \in \mathscr{V}(K),\, K' \in \mathscr{B}\right) \right\}. \tag{23}$$

More precisely, in case of our four-equation model, we first check for positivity of the total density ρ_{tot}, the mass fraction Y_k for phase $k = 1,2$ and pressure P at each degree of freedom in the cell, that is, if the cell K fulfils the

– Physical Admissibility Detection criteria

$$\mathrm{PAD}_K = \begin{cases} 1 \text{ if } & \forall \sigma \in K,\ \rho_{tot,\sigma}^{\star,n+1} < 0 \text{ or } Y_{1,\sigma}^{\star,n+1} < 0 \\ 0 \text{ else.} \end{cases} \tag{24}$$

To prevent the numerical approximation to be Not-A-Number (NaN) or Infinity (Inf), we perform the check via the

– Computational Admissibility Detection criteria

$$\mathrm{CAD}_K = \begin{cases} 1 \text{ if } & \exists \sigma \in K,\ U_\sigma^{\star,n+1} = \mathrm{NaN} \text{ or } U_\sigma^{\star,n+1} = \mathrm{Inf}, \\ 0 \text{ else.} \end{cases} \tag{25}$$

In case we are within a plateau area, we make sure to not break that area by applying a

– Plateau Detection criteria

$$\mathrm{P}_K = \begin{cases} 0 \text{ if } & \exists \sigma \in K, \quad |M^n - m^n| \geq \mu^3, \\ 1 \text{ else.} \end{cases} \tag{26}$$

The bounds are defined by

$$M^n = \max_{K' \in \mathscr{V}(K), \sigma \in K'} (U_\sigma^n), \qquad m^n = \min_{K' \in \mathscr{V}(K), \sigma \in K'} (U_\sigma^n), \tag{27}$$

where the neighbourhood $\mathscr{V}(K)$ is the set of cells surrounding K, and the relaxed parameter is given by $\mu = |K|^{1/d}$, with d the size of the considered dimensions within our problem set.

Finally, to prevent the approximation from numerical oscillations we adopt the

– Numerical Admissibility Detection criteria

$$\mathrm{NAD}_K = \begin{cases} 1 \text{ if } & \mathrm{DMP}_K = 1 \text{ and } \mathrm{SE}_K = 1 \\ 0 \text{ else.} \end{cases} \tag{28}$$

This criteria has two major steps: in case the first one is activated, only the second one will allow to state whether the cell is troubled at all or not. The first one is a so-called

1. Relaxed Discrete Maximum Principle (DMP) criteria

$$\mathrm{DMP}_K = \begin{cases} 0 \text{ if } & m^n < U_\sigma^{\star,n+1} < M^n \\ 1 \text{ else,} \end{cases} \tag{29}$$

In case the cell is marked with $\mathrm{DMP}_K = 1$, we change scheme to a more dissipative one.

3.3 A conservative approach for the non-conservative formulation

In order to solve 14, the scheme applied to the non-conservative equation has to be modified appropriately. In the present work, following [5], to treat the equation written in terms of the internal energy

$$\frac{\partial e_{tot}}{\partial t} + \mathbf{u} \cdot \nabla e_{tot} + (e_{tot} + P) \text{ div } \mathbf{u} = 0, \tag{30}$$

the Rusanov scheme is re-designed as

$$\begin{aligned} \phi_{\sigma,e}^{K,Rus} = \frac{1}{N_{DoF}} \int_K \left(\frac{e_{tot,h}^{(n,m)} - e_h^{n,0}}{\Delta t_{n,m}} + u_h \cdot \nabla e_h + (e_h + P_h) \text{ div } u_h \right) d\mathbf{x} \\ + \alpha_K \big(\frac{e_\sigma^{(n,m)} - e_\sigma^{n,0}}{2} - \bar{e}_K \big). \end{aligned} \tag{31}$$

For simplicity we are assuming hereafter by e the total internal energy, having dropped the subscript tot.

One may observe that (31) does not preserve the conservation of the total energy. To allow the method to get relevant weak solutions, the residual of the internal energy of (31) is corrected via

$$\widetilde{\phi_{\sigma,e}^{K,Rus}} = \phi_{\sigma,e}^{K,Rus} + r_\sigma^K \tag{32}$$

i.e. it is recast as

$$\begin{aligned} \sum_{\sigma \in K} \phi_{\sigma,e}^{K,Rus} + \sum_{\sigma \in K} r_\sigma^K = \phi^{E,K} - \sum_{\sigma \in K} \frac{\mathbf{u}_\sigma^{n,m+1} + \mathbf{u}_\sigma^{n,m}}{2} \cdot \phi_{\sigma \mathbf{m}}^{K,Rus} \\ + \frac{1}{2} \sum_{\sigma \in K} \mathbf{u}_\sigma^{n,m} \cdot \mathbf{u}_\sigma^{n,m+1} \cdot \phi_{\sigma,\rho}^{K,Rus}. \end{aligned} \tag{33}$$

To summarize, the spatial approximation for both the density $\phi_{\sigma,\rho}^{K,Rus}$ and momentum equations $\phi_{\sigma,m}^{K,Rus}$ is chosen according to **??**, while the energy is approximated via the $\widetilde{\phi_{\sigma,e}^{K,Rus}}$ nodal residual according to 33.

3.4 Treatment of the source terms

Once an approximation to (14) has been obtained, the solution is corrected by adding the sources terms (15). Let us start by doing some considerations on the source $\Gamma = \theta(g_l - g_g)$. We assume, in general, to have vaporization, in case a cell contains a non-negligible quantity of a phase and the Gibbs free energy g_1 of, for instance, the liquid media is greater than the one of the gaseous media g_2. On the contrary, liquefaction is due to a Gibbs free energy of the gaseous media greater than the one of the liquid

one. In these two specific cases, the relaxation time θ is considered to be ∞. Else, in case no mass transfer is accounted, $\theta = 0 = \Gamma$.

Following [20], we denote hereafter by superscript 0 the result obtained from the approximation of the hyperbolic system (14) and by $\star$ the one linked to the mass transfer (15). Clearly, even during the mass transfer, the conservation of the density, momentum and energy need to be preserved, i.e.

$$\begin{cases} \rho_{tot}^0 = \rho_{tot}^\star, \\ (\rho_{tot} u)^0 = (\rho_{tot} u)^\star, \\ e_{tot}^0 = e_{tot}^\star. \end{cases} \tag{34}$$

Through the relations $\rho_{tot}^0 = \alpha_l^* \rho_l^* + \alpha_g^* \rho_g^*$ and $e_{tot}^0 = \alpha_l^* e_l^* + \alpha_g^* e_g^*$ it is possible to obtain a formulation that links the pressure to the temperature.

Indeed, considering (7) along the thermodynamic closure (6), one obtains a quadratic expression that links the pressure to the temperature, s.t.

$$\begin{aligned} &a_p(P^*)(T^*)^2 + b_p(P^*)T^* + d_p(P^*) = 0, \\ &a_p(P^*) = \rho_{tot}^0 C_{vl} C_{vg}((\gamma_g - 1)(P^* + \gamma_l P_{\infty,l}) - (\gamma_l - 1)(P^* + \gamma_g P_{\infty,g}), \\ &b_p(P^*) = e^0((\gamma_l - 1)C_{vl}(P^* + P_{\infty,g}) - (\gamma_g - 1)C_{vg}(P^* + P_{\infty,l})) \\ &\qquad + \rho^0((\gamma_g - 1)C_{vg} q_l (P^* + P_{\infty,l} - (\gamma_l - 1)C_{vl} q_g (P^* + P_{\infty g})), \\ &\qquad + C_{vg}(P^* + P_{\infty,g})(P^* + \gamma_g P_{\infty,g}) - C_{vl}(P^* + P_{\infty,l})(P^* + \gamma_l P_{\infty,l}), \\ &d_p(P^*) = (q_g - q_g)(P^* + P_{\infty,l})(P^* + P_{\infty,g}). \end{aligned} \tag{35}$$

Using the condition of thermochemical equilibrium $g_l^* = g_g^*$ for a stiffened gas equation of state and two phases one obtains the pressure-temperature saturation curve that reads

$$\begin{aligned} \frac{C_{pl} - C_{pg} + q_g^{'} - q_l^{'}}{C_{pg} - C_{v_l}} + \frac{1}{T}\frac{q_l - q_g}{C_{pg} - C_{vg}} + \frac{C_{pg} - C_{pl}}{C_{pg} - C_{vg}} log T \\ + \frac{C_{pl} - C_{vl}}{C_{pg} - C_{vg}} log(P + P_{\infty,l}) - log(P + P_{\infty,g}) = 0. \end{aligned} \tag{36}$$

The equation (36) is non-linear and can be solved for the pressure, for example, by using the Newton-Rhapson Method.
Since one obteins from (36) the pressure, it is possible to obtain from (35) the corresponding value of the temperature and take the physically admissible solution of the two resulting roots. See [20] for more details.

4 Conservative wave propagation scheme

In order to cross-validate the four-equation model, we solve the conservative system (1) through a wave propagation scheme implemented within the CLAWPACK software

[17]. This approach is based on an alternative formulation of the Godunov scheme, namely the wave propagation formulation

$$U_\sigma^{n+1} = U_\sigma^n - \frac{\Delta t}{\Delta x}(\mathbf{A}^+ \Delta U_{\sigma-\frac{1}{2}} + \mathbf{A}^- \Delta U_{\sigma+\frac{1}{2}}) + \frac{\Delta t}{\Delta x}(\mathscr{F}_{\sigma-\frac{1}{2}} - \mathscr{F}_{\sigma+\frac{1}{2}}). \tag{37}$$

Following [20], we define the left-going and right-going fluctuations arising from Riemann problems at cell interfaces $x_{\sigma+1/2}$ as

$$A^\pm \Delta U_{\sigma+\frac{1}{2}} = \sum_l (s^l_{\sigma+\frac{1}{2}})^\pm W^l_{\sigma+\frac{1}{2}}, \tag{38}$$

where s^l is the speed at which the wave W^l propagates, $l = 1,\ldots,M$, with M denoting the number of waves of the chosen Riemann solver ($M = 3$ for the HLLC solver). Let us recall that the Riemann solution structure $\left\{ W^l_{\sigma+\frac{1}{2}}, s^l_{\sigma+\frac{1}{2}} \right\}_{l=1,2,\ldots,M}$ provided by the Riemann solver must satisfy $\Delta U = U_{\sigma+1} - U_\sigma = \sum_l W^l_{\sigma+\frac{1}{2}}$. Furthermore, for conservation laws we require $\Delta f(U) = f(U_{\sigma+1}) - f(U_\sigma) = \sum_l s^l_{\sigma+\frac{1}{2}} W^l_{\sigma+\frac{1}{2}}$.

The $\mathscr{F}_{\sigma\mp\frac{1}{2}}$ correspond to correction fluxes to achieve (formal) second-order accuracy

$$\mathscr{F}_{\sigma+\frac{1}{2}} = \frac{1}{2}\sum_l |s^l_{\sigma+\frac{1}{2}}|(1 - \frac{\Delta t}{\Delta x}|s_{\sigma+\frac{1}{2}}|)\bar{W}^l_{\sigma+\frac{1}{2}}. \tag{39}$$

Here $\bar{W}^l_{\sigma+\frac{1}{2}}$ are a limited version of the waves $W^l_{\sigma+\frac{1}{2}}$, obtained as

$$\bar{W}^l_{\sigma+\frac{1}{2}} = \phi(\theta^l_{\sigma+\frac{1}{2}}) W^l_{\sigma+\frac{1}{2}},$$

where $\phi(\theta)$ is a limiter function. The smoothness indicator θ can be defined as:

$$\theta^l_{\sigma+\frac{1}{2}} = \frac{W^l_{I+\frac{1}{2}} \cdot W^l_{\sigma+\frac{1}{2}}}{W^l_{\sigma+\frac{1}{2}} \cdot W^l_{\sigma+\frac{1}{2}}},$$

where $I = \sigma - 1$ if $s^l_{\sigma+\frac{1}{2}} > 0$ and $I = \sigma + 1$ if $s^l_{\sigma+\frac{1}{2}} < 0$. Here a Minmod limiter is used, $\phi(\theta) = \max(0, \min(1, \theta))$

In order to define the fluctuations $A^\pm \Delta U_{\sigma+\frac{1}{2}}$, i.e. to retrieve the Riemann solution structure $\left\{ W^l_{\sigma+\frac{1}{2}}, s^l_{\sigma+\frac{1}{2}} \right\}_{l=1,2,\ldots,M}$, we chose a HLLC-type solver, which was first proposed in [24]. Let us consider a Riemann problem with left and right data U_L and U_R, respectively. The HLLC solver consists of $M = 3$ waves W^l moving at speeds $s^1 = S_L$, $s^2 = S^\star$ and $s^3 = S_R$, and separating four constant states U_L, $U_L^\star$, $U_R^\star$ and U_R, as shown in Figure 5.

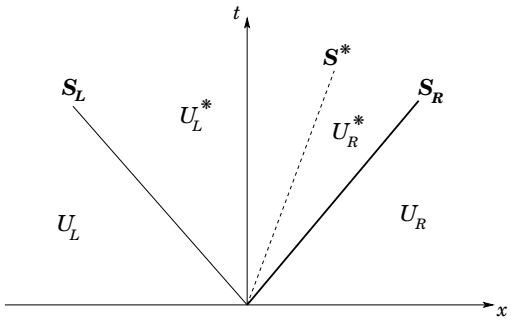

Fig. 5 Representation of the wave structure given by a Riemann problem. Each non-linear wave represented respectively by S_L, $S^\star$ and S_R represents a discontinuity.

Following [12], we define the speed $S_L = \min\left((u-c_{tot})_R,(u-c_{tot})_L\right)$, $S_R = max((u+c_{tot})_R,(u+c_{tot})_L)$ and

$$S^\star = u^\star = \frac{P_R - P_L + \rho_{tot_L} u_L(S_L-u_L) - \rho_{tot_R} u_R(S_R-u_R)}{\rho_{tot_L}(S_L-u_L) - \rho_{tot_R}(S_R-u_R)}.$$

Furthermore, in order to obtain the middle states $U_L^\star$ and $U_R^\star$ for the (1), we follow [22]. Setting $\xi = L,R$, we write

$$U_\xi^\star = \begin{cases} \rho_{tot_\xi}^\star = \rho_{tot_\xi} \frac{u_\xi - S_\xi}{S^star - S_\xi}, \\ u_\xi^\star = u^\star = S^\star, \\ P_\xi^\star = P_\xi + \rho_{tot_\xi}\left(u_\xi - S_\xi\right)\left(u_\xi - S^\star\right), \\ E_{tot_\xi}^\star = E_{tot_\xi} + \frac{P_\xi\left(u_\xi - S^\star\right)}{\rho_\xi\left(u_\xi - S_\xi\right)} - S^\star\left(u_\xi - S^\star\right), \\ Y_{k_\xi}^\star = Y_{k_\xi}. \end{cases} \tag{40}$$

These relations allow us to define, for example, the flux via the Rankine–Hugoniot relations, such that $F_\xi^\star = F_\xi - S_\xi(U_\xi - U_\xi^\star)$. Finally, the waves for the HLLC solver are defined as $W^1 = U_L^\star - U_L$, $W^2 = U_R^\star - U_L^\star$ and $W^3 = U_R - U_R^\star$.

5 Numerical Results

Hereafter, we present different benchmark problems taken from literature. In particular, the assessment of the results will be done by comparing the presented Residual Distribution scheme in non-conservative form and the HLL solver applied to a model written in the classical conservative form. We systematically consider stiffened gas equations of state.

5.1 1D Shock Tube Test for a Liquid-Vapour Mixture

The first considered benchmark problem, is the one presented in Chiapolino et al. [10]. This test constitutes in a shock tube with liquid and vapour water in a mixed state. Initially, left and right of the diaphragm, there is an equal amount of this mixture, with a predominant water vapour volume fraction and an initial state of the two phases according to Table 1.

The conditions in the shock tube problem are initialized with the same velocity $u_L = u_R = 0$m/s, where the subscripts L and R denote respectively left and right of the diaphragm. The temperatures are set to $T_L = 394.2489$K and $T_R = 372.8827$K and the pressures to $P_L = 2 \cdot 10^5$Pa and $P_R = 1 \cdot 10^5$Pa.

Note, that in [10] the initial data has been provided considering the saturation temperature for the two states calculated via the Gibb's enthalpy equality. Using the q' according to [10], the temperature and density result to be overestimated, therefore, in this benchmark problem, we have considered the q' from [20].

Phase	Fluid	Y_1	$c_v\ [\frac{J}{kgK}]$	γ	$P_\infty\ [Pa]$	$q\ [\frac{J}{kg}]$	$q'\ [\frac{J}{kgK}]$
1	Liquid	0.2	1816	2.35	$1 \cdot 10^9$	$-1167 \cdot 10^3$	0
2	Gas	0.8	1040	1.43	0	$2030 \cdot 10^3$	$-23.4 \cdot 10^3$

Table 1 Initial fluid properties and parameters of the water liquid and vapour phases for the problem of Section 5.1.

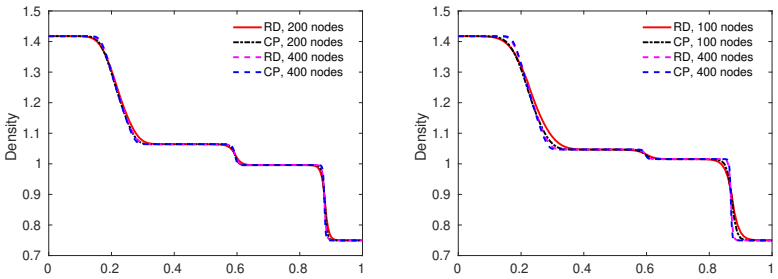

Fig. 6 Shock tube test with a mixture containing mainly water vapour at $t = 0.8$ms. Comparison of the density for the non-conservative RD formulation and the conservative CLAWPACK (CP) approach on different mesh sizes - *without* mass transfer (left) and *with* mass transfer (right).

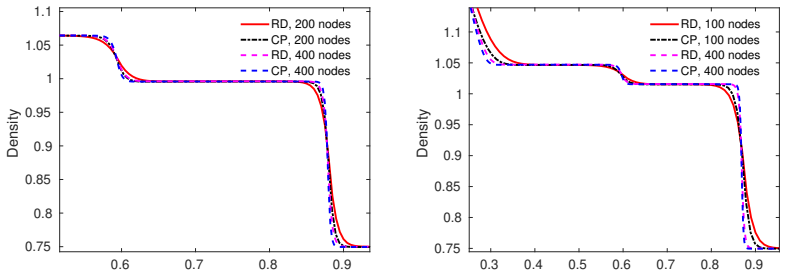

Fig. 7 Shock tube test with a mixture containing mainly water vapour at $t = 0.8$ms. Details of the density plots of Figure 8 for the non-conservative RD formulation and the conservative CLAWPACK (CP) approach on different mesh sizes - *without* mass transfer (left) and *with* mass transfer (right).

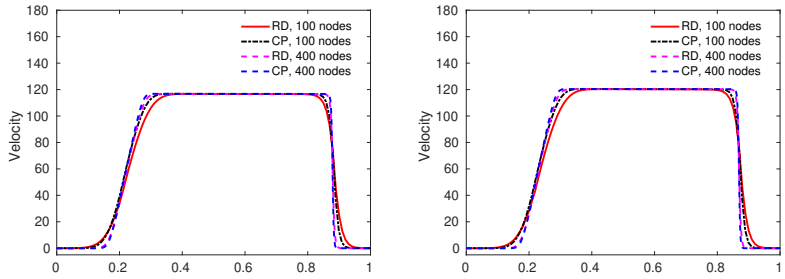

Fig. 8 Shock tube test with a mixture containing mainly water vapour at $t = 0.8$ms. Comparison of the velocity for the non-conservative RD formulation and the conservative CLAWPACK (CP) approach on different mesh sizes - *without* mass transfer (left) and *with* mass transfer (right).

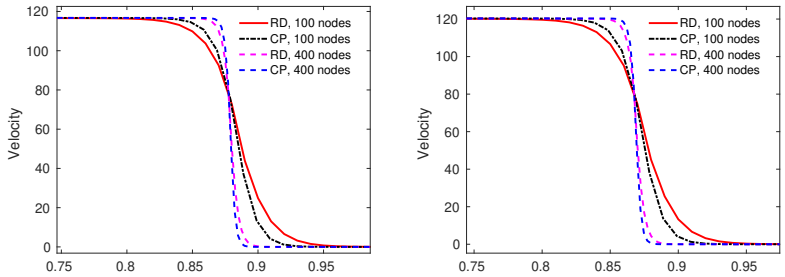

Fig. 9 Shock tube test with a mixture containing mainly water vapour at $t = 0.8$ms. Details of the velocity plots of Figure 8 for the non-conservative RD formulation and the conservative CLAWPACK (CP) approach on different mesh sizes - *without* mass transfer (left) and *with* mass transfer (right).

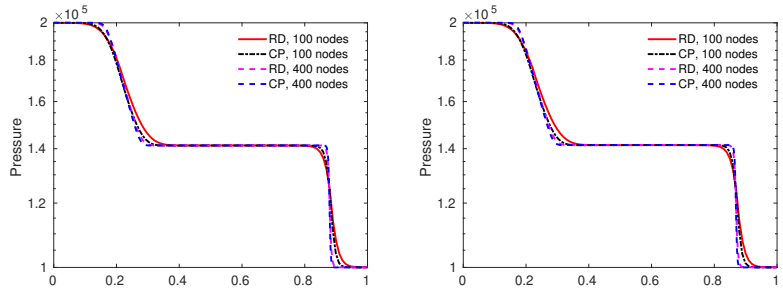

Fig. 10 Shock tube test with a mixture containing mainly water vapour at $t = 0.8$ms. Comparison of the pressure for the non-conservative RD formulation and the conservative CLAWPACK (CP) approach on different mesh sizes - *without* mass transfer (left) and *with* mass transfer (right).

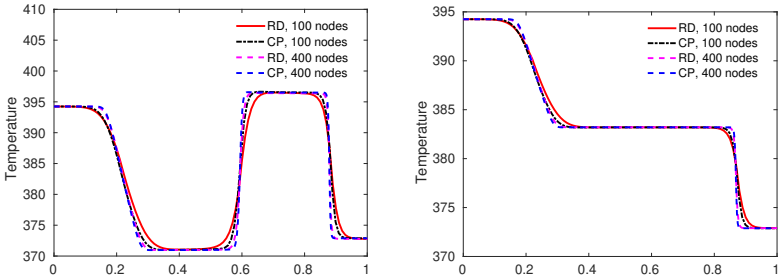

Fig. 11 Shock tube test with a mixture containing mainly water vapour at $t = 0.8$ms. Comparison of the temperature for the non-conservative RD formulation and the conservative CLAWPACK (CP) approach on different mesh sizes - *without* mass transfer (left) and *with* mass transfer (right).

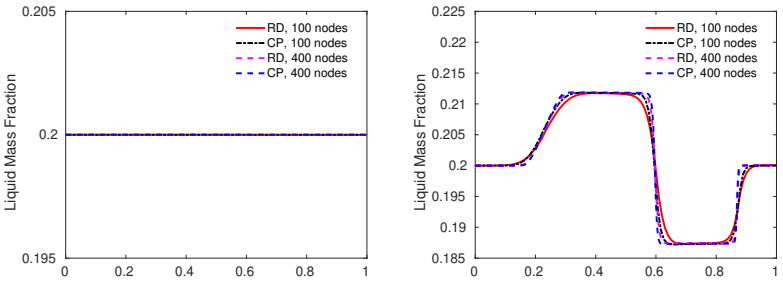

Fig. 12 Shock tube test with a mixture containing mainly water vapour at $t = 0.8$ms. Comparison of the liquid mass fraction for the non-conservative RD formulation and the conservative CLAWPACK (CP) approach on different mesh sizes - *without* mass transfer (left) and *with* mass transfer (right).

In the following, we have compared the non-conservative RD method along with the conservative given by the CLAWPACK (CP) solver an the results are shown in Figures 6-12. In particular, we have considered on the left side of each figure the approximation to the hyperbolic problem (14) and on the right hand side the system (15), which includes the mass transfer. The obtained results show an excellent overlap of the non-conservative formulation via the RD method and the conservative one via the CP solver, in particular across each interacting discontinuity, and throughout any mesh refinement.

5.2 2D Shock Tube Test for a Liquid-Vapour Mixture

We now consider the 2D extension of the previous test-case. We assume a solid wall both on the top and the bottom boundary of the tube.

We have considered two meshes, and both constituted of uniform quadrangles: one of 100x10 meshes and one of 200x20 meshes. The results are reported in Figure 13. There is good agreement between the results with the RD and FV methods. There are no parasitic oscillations along the y-axis. However, some oscillations can be noted at the contact discontinuity. Note that the RD method captures the shocks with a better resolution than FV, especially thanks to the a-posteriori algorithm.

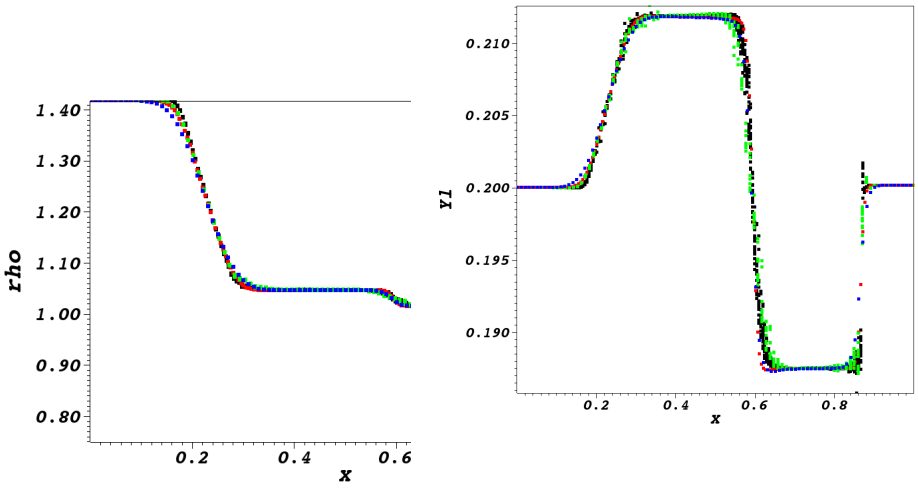

Fig. 13 Profil de la densité ρ (à gauche) et de la fraction massique de liquide Y_l (à droite) d'un tube à choc eau-vapeur en 2D (noir : 200x20 nœuds rd, rouge : 200x20 nœuds Clawpack, vert : 100x10 nœuds rd, bleu : 100x10 nœuds Clawpack)

5.3 Depressurisation of a Pipe with Pure CO_2

As a further test problem, we have considered the depressurization of a pipe with pure CO_2, following the benchmark problem proposed in [19]. At $x = 50$m within a domain of total length $L = 80$m, we set a discontinuity in a pipe. The conditions on the left and right of x are in terms of pressures $P_L = 60 \cdot 10^5$Pa and $P_R = 10 \cdot 10^5$Pa, with an initial velocity $u_L = u_R = 0$m/s, a temperature $T_L = T_R = 273K$ and a volume fraction for the liquid phase $\alpha_L = 0.99999$ and the gaseous one $\alpha_R = 10^{-5}$. The initial fluid properties parameters are shown in detail in Table 2. Since the original reference paper of this benchmark problem does not explicitly write all the considered parameters, we have chosen some parameters with freedom, as the volume fraction, the Gibb's enthalpy, as well as q', as reported in Table 2.

Phase	Fluid	$c_v\ [\frac{J}{kgK}]$	γ	$P_\infty\ [Pa]$	$q\ [\frac{J}{kg}]$	$q'\ [\frac{J}{kgK}]$
1	Liquid	$2.44 \cdot 10^3$	1.23	$1.32 \cdot 10^8$	$-6.23 \cdot 10^5$	$-5.3409289 \cdot 10^3$
2	Gas	$2.41 \cdot 10^3$	1.06	$8.86 \cdot 10^5$	$-3.01 \cdot 10^5$	$-1.0398090 \cdot 10^4$

Table 2 Initial fluid properties and parameters for the pure CO_2 for Section 5.3.

The results hereafter are shown at time $t = 0.08$s. We note, that, contrary to [19], we have considered within this test case only the mass transfer due to evaporation. Indeed, in [19], this benchmark problem has been tested using evaporation and liquefaction. We have obtained an excellent agreement between the non-conservative RD approximations and the CLAWPACK ones, as shown in Figures 14 and 18 for the case without mass transfer and in Figures 19 and 23 for the system with mass transfer. In particular, throughout the Figures showing various zooms of the considered physical quantities, one can see, how the two solutions mostly overlap and converge towards the same solution.

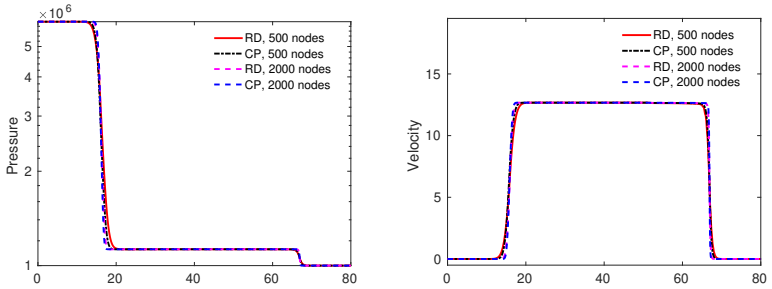

Fig. 14 Depressurisation of a pipe with pure CO_2 at $t = 0.08$s. Comparison between the non-conservative RD and the conservative CLAWPACK (CP) approximation on different mesh sizes *without* mass transfer - pressure (left) and velocity (right).

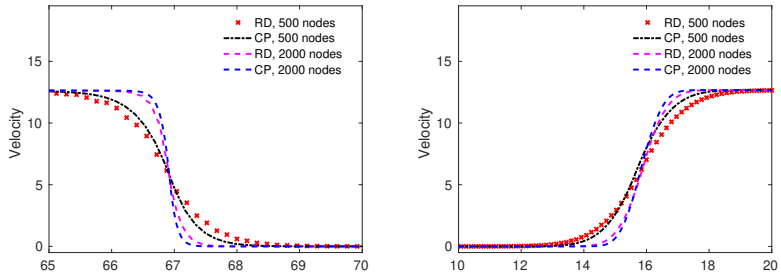

Fig. 15 Depressurisation of a pipe with pure CO_2 at $t = 0.08$s. Comparison between the non-conservative RD and the conservative CLAWPACK (CP) approximation on different mesh sizes for the system *without* mass transfer - velocity zooms.

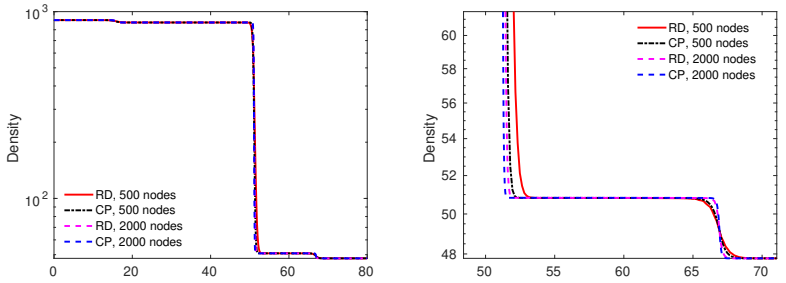

Fig. 16 Depressurisation of a pipe with pure CO_2 at $t = 0.08$s. Comparison between the non-conservative RD and the conservative CLAWPACK (CP) approximation on different mesh sizes *without* mass transfer - density (left) and density zoom (right).

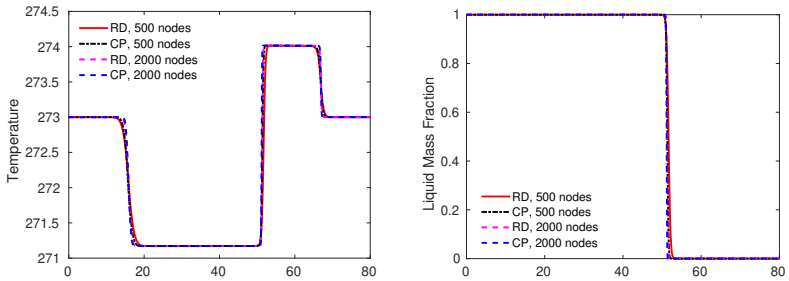

Fig. 17 Depressurisation of a pipe with pure CO_2 at $t = 0.08$s. Comparison between the non-conservative RD and the conservative CLAWPACK (CP) approximation *without* mass transfer - temperature (left) and liquid mass fraction (right).

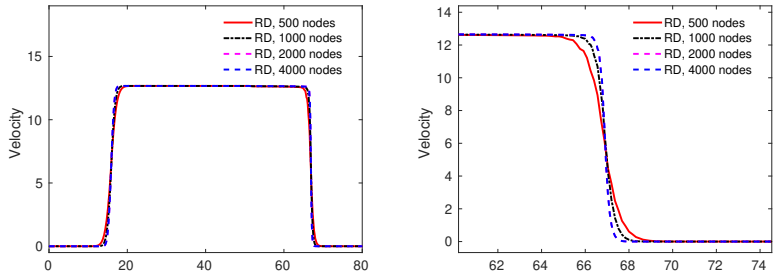

Fig. 18 Depressurisation of a pipe with pure CO_2 at $t = 0.08$s. Mesh convergence study for the non-conservative RD *without* mass transfer - velocity (left) and its zoom (right).

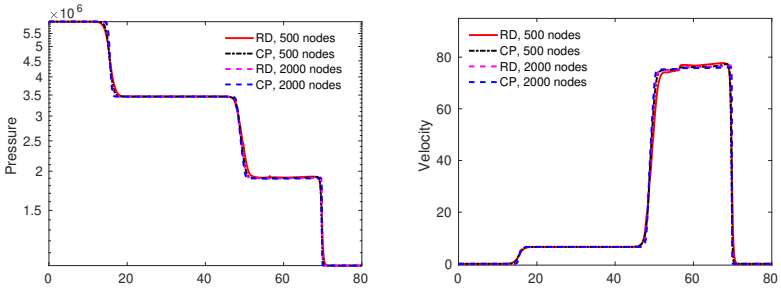

Fig. 19 Depressurisation of a pipe with pure CO_2 at $t = 0.08$s. Mesh convergence study for the non-conservative RD *with* mass transfer - pressure (left) and velocity (right).

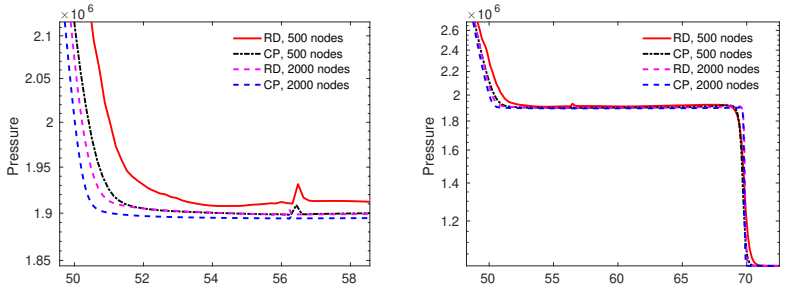

Fig. 20 Depressurisation of a pipe with pure CO_2 at $t = 0.08$s. Mesh convergence study for the non-conservative RD for the system *with* mass transfer - pressure zooms.

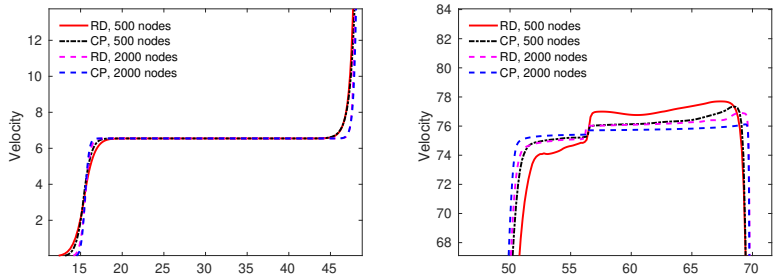

Fig. 21 Depressurisation of a pipe with pure CO_2 at $t = 0.08$s. Mesh convergence study for the non-conservative RD for the system *with* mass transfer - velocity zooms.

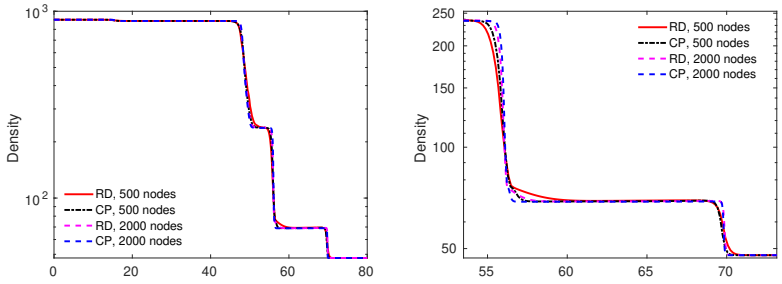

Fig. 22 Depressurisation of a pipe with pure CO_2 at $t = 0.08$s. Mesh convergence study for the non-conservative RD for the system *with* mass transfer - density (left) and density zoom (right).

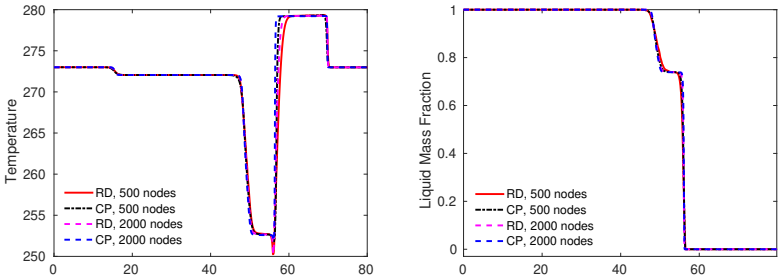

Fig. 23 Depressurisation of a pipe with pure CO_2 at $t = 0.08$s. Mesh convergence study for the non-conservative RD for the system *with* mass transfer - temperature (left) and liquid mass fraction (right).

5.4 Cavitation Test for Water

In the context of the considered reduced Baer- and Nunziato models, a well established benchmark problem to assess the robustness of the an approach is given by so-called water cavitation tube tests (see e.g. [23,20]). Let us consider a discontinuity set at $x = 0.5$m within our domain of length $L = 1$m and initial velocity left and right from the discontinuity to be $u_L = -2$m/s and $u_R = 2$m/s. Further, we set for the liquid a density $\rho_{liq} = 1150$ [kg/m^3] and for the vapour $\rho_{vap} = 0.63$ [kg/m^3]. The liquid volume fraction is set to $\alpha_{vap} = 0.01$. The pressure at the initial time is $P = 10^5$ [Pa] and the temperature $T = 354.728$ [K]. The parameters used within the stiffened equations of state are taken according to Table 1.
Comparing the CLAWPACK and the RD approximations, as shown in Figures 24-31, both approximation appear to be in perfect agreement and overlap good.

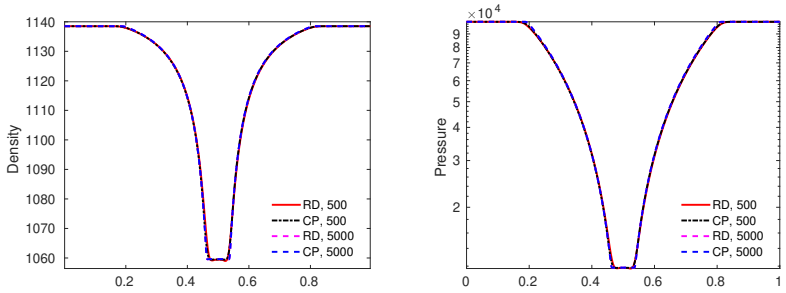

Fig. 24 Water cavitation tube problem for $|u| = 2$m/s at $t = 3.2$ms. Comparison of the RD formulation with the CLAWPACK (CP) solution on different mesh sizes *without* mass transfer for density (left) and pressure (right).

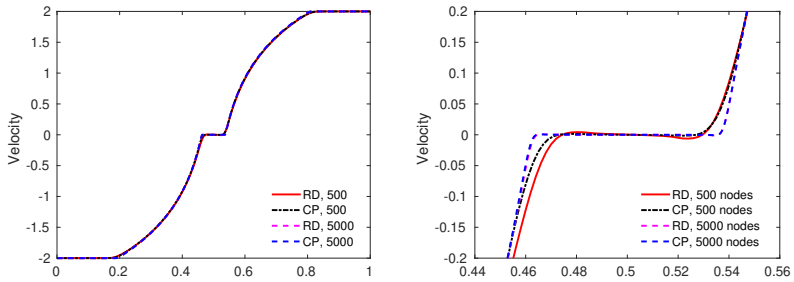

Fig. 25 Water cavitation tube problem for $|u| = 2$m/s at $t = 3.2$ms. Comparison of the RD formulation with the CLAWPACK (CP) solution on different mesh sizes *without* mass transfer - velocity (left) and zoom of the velocity (right).

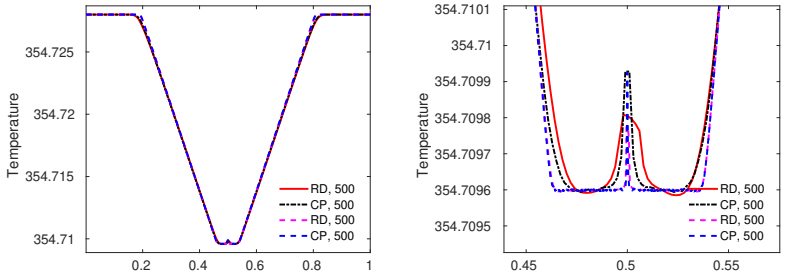

Fig. 26 Water cavitation tube problem for $|u| = 2$m/s at $t = 3.2$ms. Comparison of the RD formulation with the CLAWPACK (CP) solution on different mesh sizes *without* mass transfer - temperature (left) and zoom of the temperature (right).

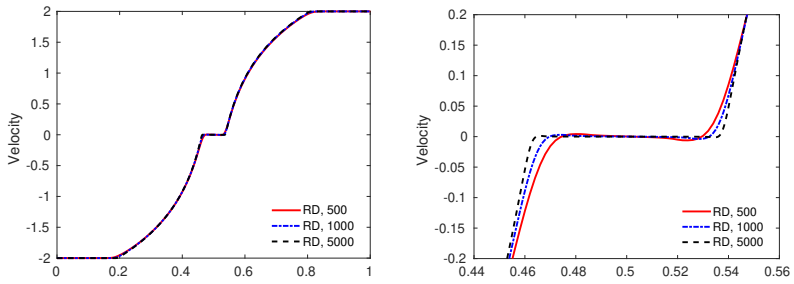

Fig. 27 Water cavitation tube problem for $|u| = 2$m/s at $t = 3.2$ms. Mesh convergence of the RD formulation *without* mass transfer - velocity (left) and zoom of the velocity (right).

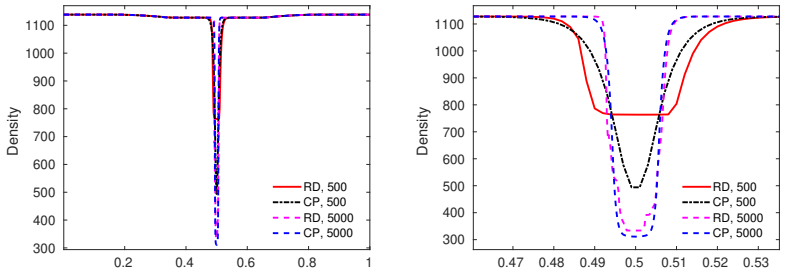

Fig. 28 Water cavitation tube problem for $|u| = 2$m/s at $t = 3.2$ms. Comparison of the RD formulation with the CLAWPACK (CP) solution on different mesh sizes *with* mass transfer - density (left) and density zoom (right).

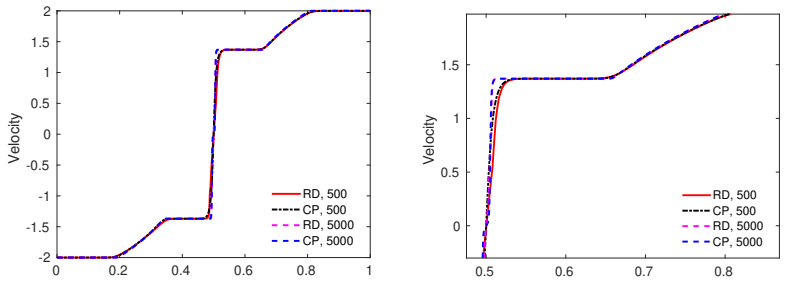

Fig. 29 Water cavitation tube problem for $|u| = 2$m/s at $t = 3.2$ms. Comparison of the RD formulation with the CLAWPACK (CP) solution on different mesh sizes *with* mass transfer - velocity (left) and veocity zoom (right).

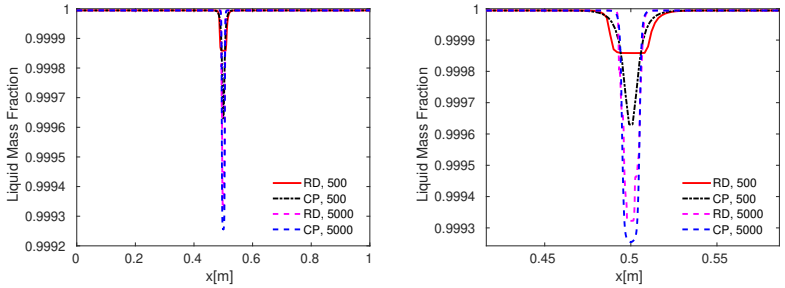

Fig. 30 Water cavitation tube problem for $|u| = 2$m/s at $t = 3.2$ms. Comparison of the RD formulation with the CLAWPACK (CP) solution on different mesh sizes *with* mass transfer - liquid mass fraction (left) and liquid mass fraction zoom (right).

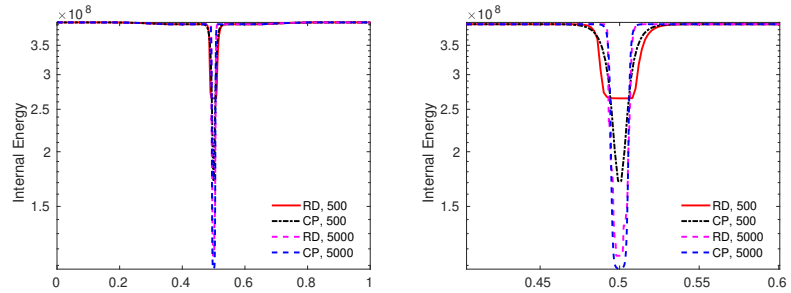

Fig. 31 Water cavitation tube problem for $|u| = 2$m/s at $t = 3.2$ms. Comparison of the RD formulation with the CLAWPACK (CP) solution on different mesh sizes *with* mass transfer - internal energy (left) and internal energy zoom (right).

5.5 Cavitation Test at High Speeds for Water

Finally, we consider a variant of the test of Section 5.4, which considers the same initial parameters of the involved fluids (see Table 1), but considers an extremely strong initial condition with $u_L = -100$m/s and $u_R = 100$m/s. Since the non-conservative term depends of the divergence of the speed, this last test case is an excellent indicator to assess the robustness of the non-conservative formulation. Indeed, while the non-conservative solution has been obtained via a CFL$= 0.2$, which coincides with the CFL used throughout all the previous benchmark problems, the conservative CLAWPACK solver requires a huge decrease of the CFL number to allow to retain a solution and not fail the computations. For the approximations with and without the mass transfer, both the RD and the CLAWPACK methods, with the opportune adjustments for the last solver, output a solution shown in Figures 32-35 that provide an overall good agreement.

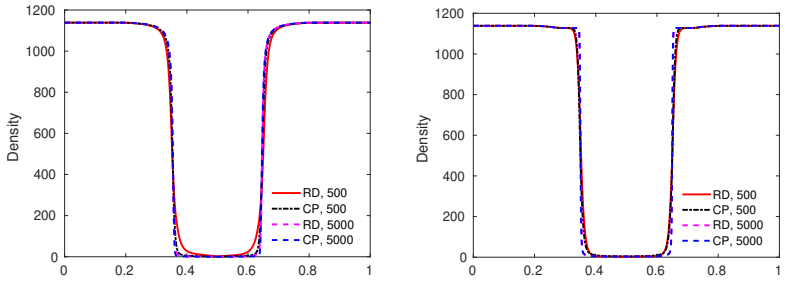

Fig. 32 Water cavitation tube problem for $|u| = 100$m/s at $t = 1.5$ms. Density: Comparison of the RD formulation with the CLAWPACK (CP) solution on different mesh sizes - *without* mass transfer (left) and *with* mass transfer (right).

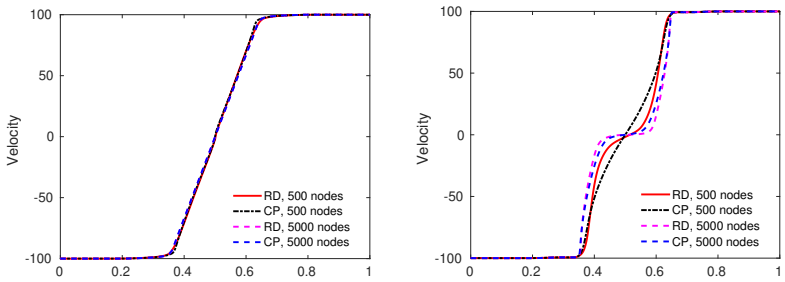

Fig. 33 Water cavitation tube problem for $|u| = 100$m/s at $t = 1.5$ms. Velocity: Comparison of the RD formulation with the CLAWPACK solution on different mesh sizes - *without* mass transfer (left) and *with* mass transfer (right).

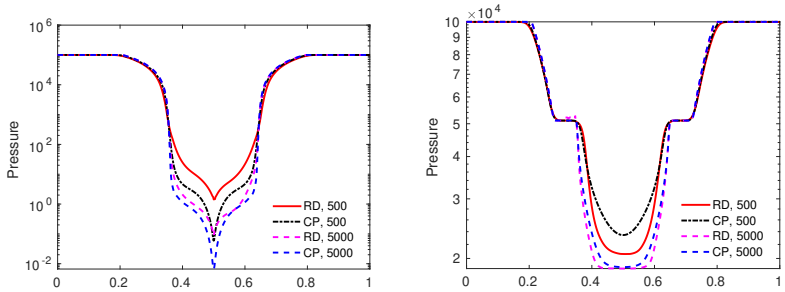

Fig. 34 Water cavitation tube problem for $|u| = 100$m/s at $t = 1.5$ms. Pressure: Comparison of the RD formulation with the CLAWPACK solution on different mesh sizes - *without* mass transfer (left) and *with* mass transfer (right).

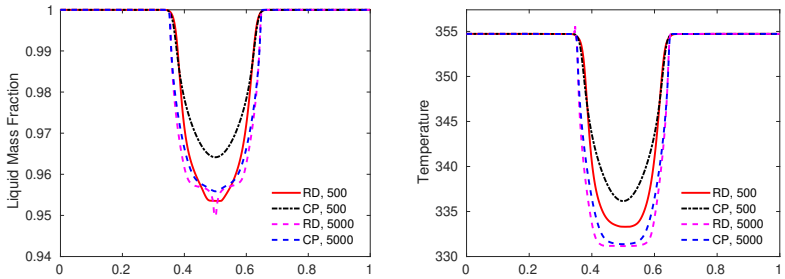

Fig. 35 Water cavitation tube problem for $|u| = 100$m/s at $t = 1.5$ms. Comparison of the RD formulation with the CLAWPACK solution on different mesh sizes with mass transfer - liquid mass fraction (left) temperature (right).

5.6 Shock Bubble Motion without Mass Transfer in 2D

In the following we consider a benchmark in 2D without considering the mass transfer terms. In particular, we have the configuration as detailed in Figure 36. On the right hand side (red area) we have initially air at a pressure $P_2 = 2.49 \cdot 10^5$Pa and velocity $u = 230.3\frac{m}{s}$. On the left, in the white area, the air is at ambient conditions, at rest, and with a pressure $P_1 = 1.013 \cdot 10^5$Pa. In this area, we have collocated a helium bubble with the same pressure as the surrounding area($P = 1.013 \cdot 10^5$Pa). The impact of the right hand side on the left hand side is comparable to a shock occurring with Mach 1.5.

Fig. 36 Sketch of the benchmark problem

We consider two cases with structured, uniform elements, with $N_1 = 24377$ and $N_2 = 54567$ elements, corresponding respectively approximately to grids of 300×80 and 450×120 cells. In Figure 37 we display the total density at $t = 577\mu s$. In particular, we compare in the upper figure the approximation optained by using CLAWPACK on a conservative formulation, i.e. (1), and the presented Residual Distribution strategy on a non-conservative set of equations, (2). The right hand side of the sytem has been neglected in this test, comparing only the hyperbolic part of the system of the four-equation model. The resulting corss-validation highlights an overall more accurate representation of the residual distribution approach, w.r.t. the Clawpack one. Nevertheless, it is possible to observe a light asymmetry in the profile of the bubble, most problably linked to the boundary conditions.

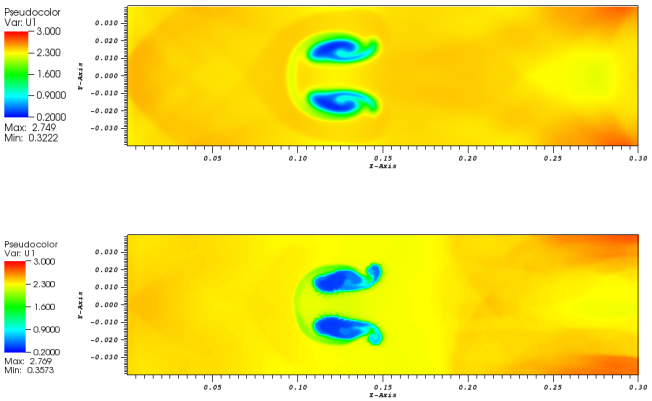

Fig. 37 upper: Clawpack solver, conservative formulation of the syste; lower: Residual Distribution method, non-conservative formulation of the system & MOOD

5.7 2D benchmark with mass transfer at $t = 0.8 \cdot 10^{-3}$s

Initial conditions

- structured grid with 79512 elements
- liquid and vapour water in mixed state
- left: $P = 2 \cdot 10^5$Pa & right: $P = 1 \cdot 10^5$Pa

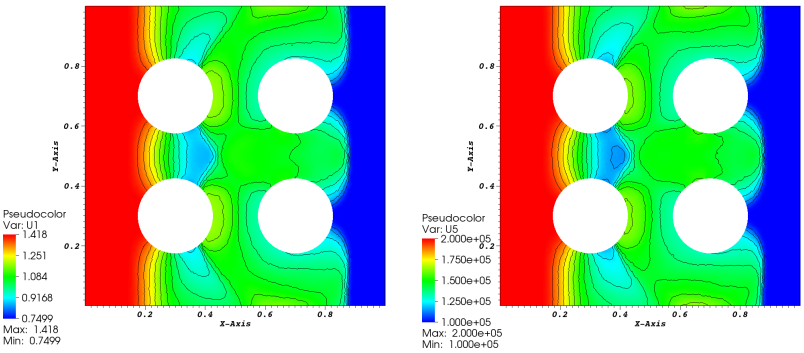

Fig. 38 upper: Clawpack solver, conservative formulation of the syste; lower: Residual Distribution method, non-conservative formulation of the system & MOOD

6 Conclusions

In this paper, we bring together the techniques presented in [8], [4], [7] and [5]. Indeed, the focus is drawn on the ability of a second-order Finite Volume based Residual Distribution scheme, written in a non-conservative form and with an "a posteriori limiting", to deal with a four-equation multiphase system with and without source terms, i.e. mass transfer. Besides testing the novel methodology on extremely severe and diverse benchmark problems, we have also tailored an HLL solver for these modelling equations written in conservative form. This has allowed to cross-validate the four-equation model via a classical Finite Volume scheme applied to a conservative formulation of the system, and via the novel Residual Distribution method for a non-conservative version of the model. The forthcoming investigations within this context will include an extension to the multidimensional case and to a higher than second-order approximation through a Finite Element based Residual Distribution method that follows the work presented in [1].

References

1. High-order Residual Distribution Scheme for the Time-Dependent Euler Equations of Fluid Dynamics. Computers & Mathematics with Applications **78**(2) (2019)
2. Abgrall, R.: Toward the Ultimate Conservative Scheme: Following the Quest. Journal of Computational Physics **167**(2), 277–315 (2001)
3. Abgrall, R.: Residual Distribution Schemes: Current Status and Future Trends. Computers and Fluids **35**(7), 641–669 (2006)
4. Abgrall, R., Bacigaluppi, P.: Design of a Second-Order Fully Explicit Residual Distribution Scheme for Compressible Multiphase Flows. In: Finite Volumes for Complex Applications VIII - Hyperbolic, Elliptic and Parabolic Problems. FVCA 2017, Springer Proceedings in Mathematics & Statistics, vol. 200. Springer, Cham (2017)
5. Abgrall, R., Bacigaluppi, P., Tokareva, S.: A High-order Nonconservative Approach for Hyperbolic Equations in Fluid Dynamics. Computers & Fluids **169**, 10–22 (2018). DOI https://doi.org/10.1016/j.compfluid.2017.08.019

6. Abgrall, R., De Santis, D., Ricchiuto, M.: High-order Preserving Residual Distribution Schemes for Advection-diffusion Scalar Problems on Arbitrary FGrids. SIAM Journal on Scientific Computing **36**(3), a955–a983 (2014). DOI 10.1137/12090143X
7. Bacigaluppi, P., Abgrall, R., Kaman, T.: Hybrid Explicit Residual Distribution Scheme for Compressible Multiphase Flows. Journal of Physics: Conference Series **821**(1) (2017)
8. Bacigaluppi, P., Abgrall, R., Tokareva, S.: "A Posteriori" Limited High Order and Robust Residual Distribution Schemes for Transient Simulations of Fluid Flows in Gasdynamics. Journal of Computational Physics In (minor) revision
9. Baer, M., Nunziato, J.: A Two-phase Mixture Theory for the Deflagration-to-detonation Transition (DDT) in Reactive Granular Materials. International journal of multiphase flow **12**(6), 861–889 (1986)
10. Chiapolino, A., Boivin, P., Saurel, R.: A Simple Phase Transition Relaxation Solver for LiquidâĂŞ-Vapor Flows. International Journal for Numerical Methods in Fluids **83**, 583–605 (2017)
11. Clain, S., Diot, S., Loubère, R.: A High-order Finite Volume Method for Systems of Conservation Laws – Multi-dimensional Optimal Order Detection (MOOD). Journal of Computational Physics **230**(10), 4028–4050 (2011)
12. Davis, S.: Simplified Second-order Godunov-type Methods. SIAM Journal on Scientific and Statistical Computing **9**(3), 445–473 (1988)
13. Deconinck, H., Ricchiuto, M.: Residual Distribution Schemes: Foundations and Analysis. In: Encyclopedia of Computational Mechanics. John Wiley & Sons, Ltd (2004)
14. Diot, S., Clain, S., Loubère, R.: Improved Detection Criteria for the Multi-dimensional Optimal Order Detection (MOOD) on Unstructured Meshes with Very High-order Polynomials. Computer & Fluids **64**, 43–63 (2012)
15. Downar-Zapolski, P., Bilicki, Z., Bolle, L., Franco, J.: The Non-equilibrium Relaxation Model for One-dimensional Flashing Liquid Flow. International journal of multiphase flow **22**(3), 473–483 (1996)
16. Le Martelot, S., Saurel, R., Nkonga, B.: Towards the Direct Numerical Simulation of Nucleate Boiling Flows. International Journal of Multiphase Flow **66**, 62–78 (2014)
17. LeVeque, R., Berger, M., et al.: CLAWPACK Software. available from netlib. att. com in netlib/pdes/claw or on the Web at the URL ftp://amath. washington. edu/pub/rjl/programs/clawpack. html (2011)
18. Lund, H.: A Hierarchy of Relaxation Models for Two-phase Flow. SIAM Journal on Applied Mathematics **72**(6), 1713–1741 (2012)
19. Lund, H., Aursand, P.: Two-phase Flow of CO2 with Phase Transfer. Energy Procedia **23**, 246–255 (2012)
20. Pelanti, M., Shyue, K.: A Mixture-energy-consistent Six-equation Two-phase Numerical Model for Fluids with Interfaces, Cavitation and Evaporation Waves. Journal of Computational Physics **259**, 331–357 (2014)
21. Ricchiuto, M., Abgrall, R.: Explicit Runge-Kutta Residual Distribution Schemes for Time Dependent Problems: Second Order Case. Journal of Computational Physics **229**(16), 5653–5691 (2010). DOI 10.1016/j.jcp.2010.04.002. URL `http://dx.doi.org/10.1016/j.jcp.2010.04.002`
22. Saurel, R., Boivin, P., Métayer, O.L.: A General Formulation for Cavitating, Boiling and Evaporating Flows. Computers & Fluids **128**, 53–64 (2016). DOI https://doi.org/10.1016/j.compfluid.2016.01.004. URL `http://www.sciencedirect.com/science/article/pii/S0045793016000153`
23. Saurel, R., Petipas, F., Abgrall, R.: Modelling Phase Transition in Metastable Liquids: Application to Cavitating and Flashing Flows. Journal of Fluid Mechanics **607**, 313–350 (2008)
24. Toro, E., Spruce, M., Speares, W.: Restoration of the Contact Surface in the Harten-Lax-van Leer Riemann Solver. Springer (1994)